J Electr Eng Technol Vol. 8, No. 4: 787-798, 2013
http://dx.doi.org/10.5370/JEET.2013.8.4.787

ISSN(Print) 1975-0102
ISSN(Online) 2093-7423

Parameter Design and Power Flow Control of Energy Recovery Power Accumulator Battery Pack Testing System

Long Bo* and Kil To Chong†

Abstract – This paper proposes a special power circuit topology and its corresponding control strategy for an energy recovery power accumulator battery pack testing system (PABPTS), which is particularly used in electric vehicles. Firstly, operation principle and related parameter design for the system are illustrated. Secondly, control strategy of the composite power converter for PABPTS is analyzed in detail. The improved scheme includes a high accuracy charge and discharge current closed loop. active power reference for the grid-side inverter is provided by the result of multiplication between battery pack terminal voltage and test current. Simulation and experimental results demonstrate that the proposed scheme could not only satisfy the requirements for PABPTS with wide-range current test, but also could recover the discharging energy to the power grid with high efficiency.

Keywords: Active power, Energy recovery, Power accumulator battery pack testing system

1. Introduction

Power accumulator battery pack test system (PABPTS), which is used to evaluate the characteristics of power battery packs, has been one of an indispensable part in the development of electric vehicles (EV). Power accumulator battery pack (PABP) must meet the test requirements for all kinds of EV under various conditions-such as during a quick starting process, climbing, accelerating, and braking. Under these conditions, PABP is required to provide an instantaneous large charging and discharging current. The comprehensive performance of the PBPTS is also critical.

Basic requirements for PBPTS have been indicated in [1, 2] and could be summarized as follows: 1. High-voltage and large-current output (such as 450V/500A, 225kW) capability. 2. Full-scope adjustable test voltage and current are allowed. 3. Time response of adjustable current which ranges from zero to the command value should be kept within 15ms, and load current should be held steady while performing an internal resistance tests. 4. High power factor on the grid side with low total harmonic distortion (THD). 5. Reversible converting ability, so that discharging energy can be recovered to the power grid with high efficiency.

There are several ways to acquire a high-resolution low-ripple discharging current. The most common method, which is still used in some products, adopts releasing energy by using high-power resistors in discharging test, hence, forces the power transistors to work in linear-region by way of gate and emitter (V_{GE}) control. The output current of the collector and emitter (I_{CE}) is proportional to V_{GE} in the linear region, this method causes a large voltage drop between collector and emitter (V_{CE}), and as a result the energy discharging current testing experiment is totally dissipated. Therefore, a power circuit for the energy recovery charging and discharging test is needed.

So far, there has been much work focused on PBPTS. In [3], a three-phase current source converter was used to evaluate the characteristics of the PBAP. A double-loop control strategy, which is based on the feedback of the grid current and the output current, was adopted. The drawbacks of this method are that the range of the power battery voltage is limited, and a large inductance is required in the power DC-link. In [3, 4], a fuzzy controller of the steady current source in the power battery testing system was used, which demonstrated that a fuzzy controller can respond quickly to the noise signal and could improve the ability of the system to resist the noise signal. In [5], Gill gave a brief description of an advanced EV/HEV battery pack testing system using an ABC-150 power system, but the topology of the power circuit still has not been published. In [6], Shikano, A. Kobayashi, H. investigated a positive electrodes after cycle testing of high-power Li-ion battery cells. In [7], Schweighofer, B and Raab, K.M obtained a battery model of a NiMH cell by using an automated test system designed to increase the speed of measurement and ensure reproducible measurement conditions. In [8], Uno, M. Tanaka, K. established a charge-discharge cycle life prediction model for super-capacitors (SCs), they pointed out that capacitance degradations were mainly influenced by temperature, thus implying that aging can be accelerated by elevating the temperature. Activation energy values of capacitance

† Corresponding Author: Advanced Electronics and Information Research Center, Departments of Electronics & Information Engineering, Chonbuk National University, Jeonju, South Korea (kitchong @chonbuk.ac.kr)
* School of Mechanical, Electronic, and Industrial Engineering, University of Electronic Science and Technology of China, Chengdu, Sichuan, China. (longbo 1978@gmail.com)
Received: June 30, 2012; Accepted: March 12, 2013

degradations were obtained from the Arrhenius equation to determine the acceleration factor. By combining the extrapolation and the acceleration factor, the cycle life prediction model was established. Their experiments indicating that the established cycle life prediction model is appropriate for SCs in alternative battery applications. In [9], A composite power circuit for PABTS has been put forward, yet, too many voltage and current sensors are used in the system, which makes the whole system complicated and expensive. Considering that the system contains a grid-connected three-phase inverter and a dc-dc buck-boost chopper, There have been many papers illustrating transformer or transformer-less grid-connected inverter system with LCL filter interface [10-14], and still some control methods and topology analysis have been presented in discussing dc-dc converter [15]. However, few papers have been found issuing on current control strategies or energy recovery control of PABPTS. Hence, based on the former works in [9], this paper will further focus on design and power control of energy recovery technology for PABPTS under high-resolution current test procedure. A simplified power flow control scheme which does not need the dc-link voltage and current sensor would be presented.

The rest of this paper is organized as follows. In section 2, composite power circuit for the PABPTS is introduced; current direction under charging and discharging mode is also exhibited separately. In section 3, design steps of the inverter side LCL filter parameter are proposed. In addition, inductance design procedure for the dc-dc converter is put forward. In section 4, control strategy of the system is explained in detail. Different from the former work in [9], minimum sensor requirement for power flow control scheme which could keep the energy to be balanced is provided. In section 5 and 6, simulations and experimental results are illustrated to demonstrate the feasibility and validity of the recommended scheme. In section 7, conclusions and future suggestions are provided based on the aforementioned sections.

2. Power Circuit Configuration

2.1 Composite power circuit design

Power circuit configuration of the grid-connected energy recovery PABPTS is shown in Fig. 1. The system is contains a bi-directional non-isolating buck-boost DC-DC converter and a bi-directional DC-AC converter. DC-DC converter is responsible for high resolution and constant current charging and discharging testing. DC-AC converter is responsible for transferring the battery energy to and from the grid. LCL interface filter is used to exhibit improved performance for high-power converters. Compared with *L* and *LC* filters, the inductance in the LCL filter required to achieve the same damping performance of the switching harmonics, and LCL filter is superior to other

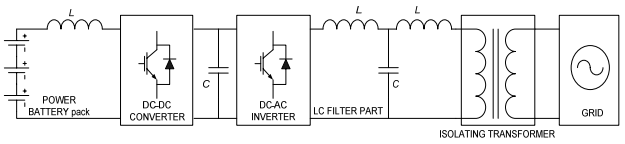

Fig. 1. Proposed power circuit for energy recovery PABPTS.

filters in attenuating high-order harmonics. Moreover, LCL filter offers less power loss due to low switching frequency of power transistors. However, this filter also introduces stability problems due to the resonance of filter inductor and capacitor. As is shown in Fig. 1, a Δ-Y isolation transformer is preferred for isolating the triplen harmonics compared with the Y-Y isolation transformer. Δ-Y type transformer could potentially achieve a relatively higher line-line voltage ratio with the same winding turn ratio, meanwhile, it could reduce costs. The drawbacks of the Δ-Y type isolation transformer are that it will cause phase drift and can reduce the ultimate gain of the open loop system by 62 % [11]. Pulse-width modulation scheme is adopted to ensure that the DC-AC VSC inverter voltage is free from low-order harmonic distortion.

Using the above arrangement, the harmonic content of the injected discharging current from the PABPTS could be well controlled at the grid side, and therefore the power quality can be greatly improved.

2.2 Operation principle of energy recovery PABPTS

Operation principle of the energy recovery PAPBTS can be divided into two ways: charging mode and discharging mode. Charging test experiment is adopted for simulation of regenerative braking of an electric vehicle, DC-link voltage is supplied by a three-phase unity power factor controlled PWM rectifier. DC-DC converter functions as a step-down chopper, and combined with proper closed-loop control, the high-resolution constant current, voltage, and power charging test needs could be realized. Current direction under this condition is shown in Fig. 2 (solid line).

Discharging test experiment is used to simulate the instantaneous driving process of an electric vehicle, it is required that PABPTS realize constant and high resolution current discharging test. In this case, the DC-DC converter functions as a step forward chopper, discharging energy charges the capacitors in the power DC-bus, thus, the reactive energy is stored in those high capacitance capacitors, which will result an increase of the voltage on

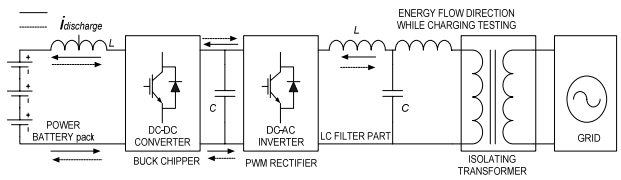

Fig. 2. Current direction of an energy recovery PABPTS in charging and discharging mode.

the DC-bus. The three-phase DC-AC inverter starts to work automatically in the case of power transistor damage caused by a high voltage on the DC bus. In addition, by using a near unity power factor grid-connected generation control strategy, the energy released from the battery will flow into the grid. Current direction in this condition mode is shown in Fig. 2 (dotted line).

3. Parameter Design of an LCL Filter

Currently, there are three kinds of filters in an grid-connected system: L, LC, and LCL filter. Compared with L and LCL filters, LCL filter has better attenuation ability when given similar size, Moreover, LCL filter could provide an inductive output at the grid interconnection point to prevent an inrush current, unlike LC or L filters. For high power output of PABPTS, power loss needs to be considered, and LCL filter requires minimum switching frequency of the power transistors. Parameters of an LCL filter are described in this section.

3.1 Mathematical model of LCL filter

Fig. 3 shows the main circuit of a LCL filter interface, where L_g and L_{inv} are the inductors associated with grid-side and inverter-side, respectively. C_f represents as the filter capacitor.

Considering about the control strategy, usually, the filter-capacitor current is used as the inner-current loop, and grid-current is measured as the outer loop variable, the inner regulator is a proportional controller, the outer regulator could choose proportional-integral (PI) controller, Fig. 4 gives the block diagram of the control loop when using grid-current as outer loop and filter capacitor current as inner loop. It could be found that the feedbacks are grid-current, capacitor current, and integral of the grid current.

Where in Fig. 4, K_p and K_i represents proportional and integral coefficient of grid-side current controller in the outer loop, respectively, while K_c stands for the proportional coefficient of inner capacitor current loop. It could be found that it is a four-order system, since an integral controller adds one order of the original three-order system. Hence, closed-loop transfer function of the system could be obtained as:

$$G(s)=\frac{i_g}{i_g^*}=\frac{A_0 s+A_1}{B_0 s^4+B_1 s^3+B_2 s^2+\left(B_3+A_0\right)s+A_1} \tag{1}$$

Where in (1), $A_0=K_p K_C$, $A_1=K_i \cdot K_c$, $B_0=L_{inv} \cdot L_g \cdot C_f$ $B_1=R_1 \cdot L_g \cdot C_f+L_{inv} \cdot C_f K_C$, $B_2=L_{inv}+L_g+R_{inv} \cdot R_g C_f+R_g \cdot C_f$, $B_3=R_{inv}+R_g$.

From (1), the characteristic equation of the closed-loop system transfer function could be shown as:

$$B_0 s^4+B_1 s^3+B_2 s^2+\left(B_3+A_0\right)s+A_1=0 \tag{2}$$

According to the Routh's stability criterion, it is needed that the coefficient of each component should be great than zero to ensure the stability of the system, then

$$\begin{cases} B_0>0, B_1>0, B_2>0, B_3+A_0>0, A_1>0 \\ B_1 B_2-B_0(B_3+A_0)>0 \\ B_1 B_2-B_0(B_3+A_0)>B_1^2 A_1/\left(B_3+A_0\right) \end{cases} \tag{3}$$

Therefore, for the given filter parameters, the grid-side current loop controller and inner capacitor current loop controller that fulfill (3) can the system be stable, yet it doesn't provide the detail accurate value of the parameters, it could be used to verify the stability of the system with the given controller parameters.

From Fig. 3, relationship between grid current i_g and inverter output voltage v_{inv} when using L and LCL filter separately, could be obtained as:

$$\begin{cases} G_{LCL}(s)=\dfrac{i_g}{u_{inv}}=\dfrac{1}{L_{inv} \cdot L_g \cdot C_f \cdot s^3+(L_{inv}+L_g) \cdot s} \\ G_L(s)=\dfrac{i_g}{u_{inv}}=\dfrac{1}{s \cdot \left(L_{inv}+L_g\right)} \end{cases} \tag{4}$$

Where in (4), u_{inv} refers inverter side voltage, i_g represents integrated grid connected current, - compared with two-order transfer function, LCL filter is a three-order system, meanwhile, L filter is an one-order system, hence, bode diagram of the two systems could be obtained and shown by using Matlab as.

It could be concluded from Fig. 5 that the output current decays with -60db/dec for LCL filter and -20db/dec for L filter at the point when the input frequency is higher than the resonant frequency. This demonstrates that LCL filter could offer better attenuation performance for higher order current harmonics.

Also seen from Fig. 5 is that both filters have the same decay frequency response with -20db/dec under low frequency input, which means that under low frequency input, LCL filter could be regarded as a pure L filter whose

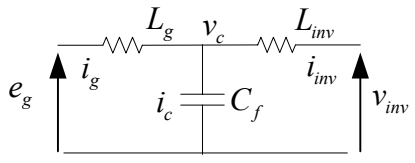

Fig. 3. Circuit topology of a LCL filter.

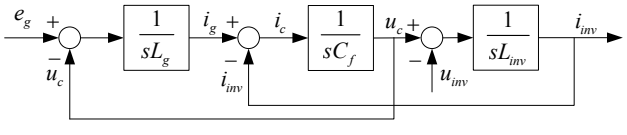

Fig. 4. Block diagram of the single-phase LCL circuit.

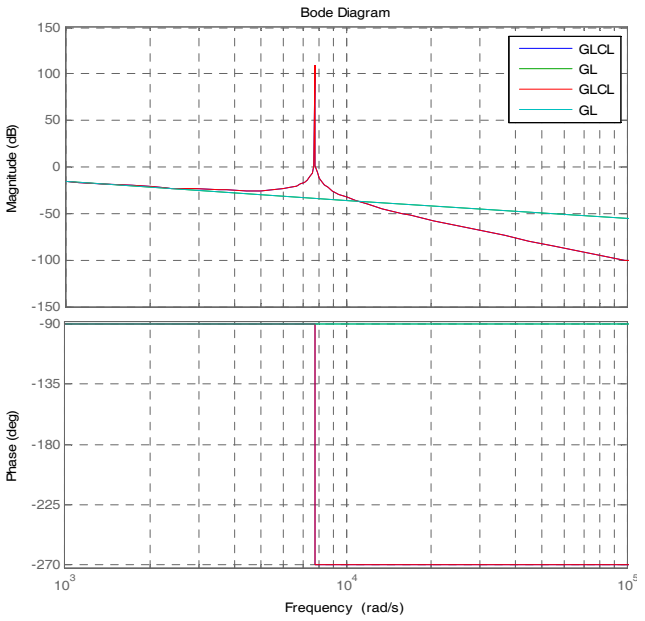

Fig. 3. Bode diagram of L and LCL filter with the same inductance.

inductance value is equal to L_{inv}+L_g. Because of their different harmonic suppression performance under high frequency input and with the same filter effect, the total inductance of a LCL filter is smaller than that of an L filter, as a result, power loss on the filter is much smaller than L filter, this explains that LCL filter would be a better choice especially when used in higher voltage and large current power converter.

3.2 Operation principle of LCL filter

Based on the transfer function of a LCL filter in (4), harmonic model could be obtained and shown in Fig. 6, transfer function between inverter side output voltage u_k and grid current i_g when expressed in $jh\omega$, would be:

$$G_{LCL} = \left|\frac{i_g(jh\omega)}{u_k(jh\omega)}\right| = \frac{1}{h\omega\left(-h^2\omega^2 L_{inv}L_g C_f + L_{inv} + L_g\right)} \quad (5)$$

Where in (5), h is the harmonic order, ω is grid frequency, from Fig. 6, the inverter side output current is decided by the grid side input inductor L_g and filter

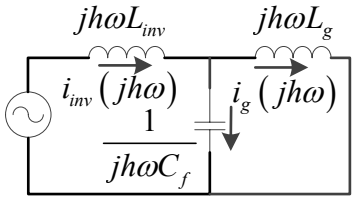

Fig. 6. Harmonic model of LCL model under grid-connected condition.

capacitor C_f, which are in parallel connected. since input impedance $X_{cf}//L_g$ is limited, moreover, the input impedance is mostly decided by the filter capacitor C_f at the switching frequency. Therefore, voltage drop of shunt impedance $X_{cf//Lg}$ would not have much influence on the inverter output current. A conclusion could be drawn that the inverter side inductor has the major influence on the current ripple.

Since, majority weight of the filter inductor is magnetic core material, a way to minimize the total weight of LCL filter, meanwhile, with the same filter performance, should be considered. Supposing the total inductance of LCL filter is L_{inv}+L_g, the ratio between them is L_{inv}/L_g, the filter capacitance is C_f, under the same filtering effect, relationship between them while $|H_{LCL}(jh\omega)|$ = 0.1, h=210, ω=100π, could be shown as:

From Fig. 7, it could be found that with the given filter performance $|H_{LCL}(jh\omega)|$ = 0.1, if the filter capacitance is chosen to be a large value, the total inductance would be

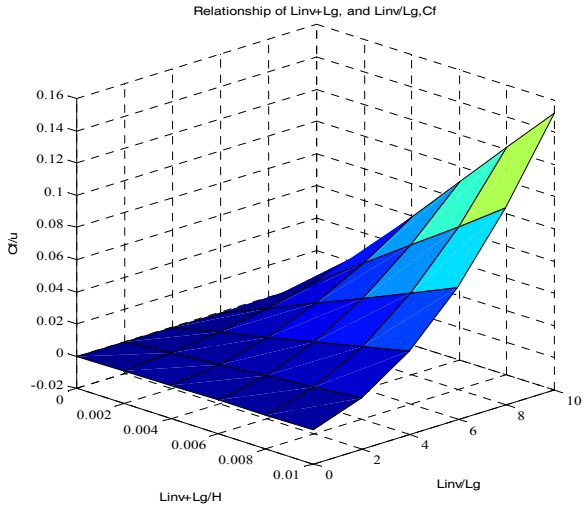

Fig. 7. Relationship diagram of L_{inv}+L_g, L_{inv}/L_g and C_f.

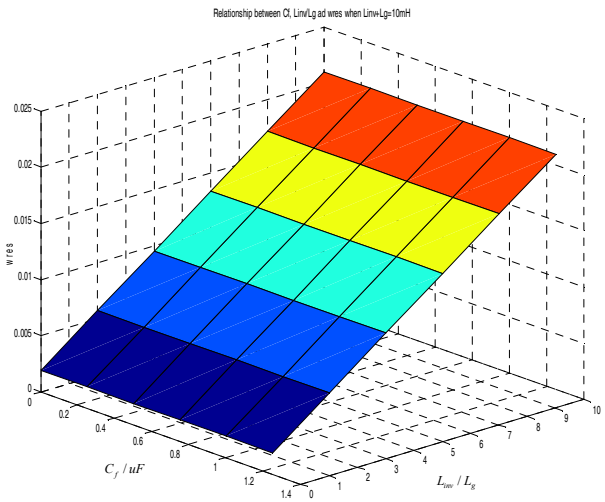

Fig. 8. Relationship between ω_{res}, L_{inv}/L_g and C_f.

reduced, correspondingly, yet, this will give an increase on L_{inv}/L_g, also seen from Fig. 7, we know that the variation of L_{inv}/L_g has less influence on the total inductance $L_{inv}+L_g$ when the filter capacitance C_f is small. Variation of L_{inv}/L_g has an obvious influence on $L_{inv}+L_g$ when the C_f is large. Fig. 8 gives the relationship between resonant frequency ω_{res} (which could calculated in (6)), L_{inv}/L_g, and C_f when $L_{inv}+L_g$ is fixed.

$$\omega_{res} = \sqrt{\frac{L_{inv} + L_g}{L_{inv} \cdot L_g \cdot C_f}} \tag{6}$$

From Fig. 8, we might see that the resonant frequency ω_{res} would decrease with the increase of filter capacitance C_f when the total filter inductance $L_{inv}+L_g$ remains constant, similarly, the resonant frequency ω_{res} would decrease when L_{inv}/L_g decrease. Small resonant frequency will make current controller design to be more difficult.

3.3 Requirements on the LCL filter design

Based on the analysis in 3.1, parameters of the LCL filter should be selected to satisfy minimum magnetic core material requirement, meanwhile, should be designed to guarantee the resonant frequency not be so small as to bring the difficulties of designing the current controller. Reference [16] gives the limitations on the parameter design of LCL filter which are listed as:

1. Voltage drop caused by the total inductance of LCL filter should no less than 10% of grid voltage under rated working conditions.
2. In order to ensure the peak value of LCL filter's resonant frequency not be appeared at low or high frequency range, the designed resonant frequency of LCL filter f_{res} should be greater than 10 times of the grid frequency, and meanwhile should be less than 1/2 of the power transistor's switching frequency, which means: $10 \cdot f_g < f_{req} < f_{sw}/2$. Resonant frequency of LCL filter is expressed as:

$$f_{res} = \frac{1}{2\pi} \sqrt{\frac{L_{inv} + L_g}{L_{inv} \cdot L_g \cdot C_f}} \tag{7}$$

To attenuate much higher frequency harmonic current, the best way is to have a shunt current which is drawn from the total power transistor switching current ripple, hence, much of the higher-order current harmonic flows to the capacitor, Which is to ensure that $X_{cf} << X_{Lg}$, where X_{cf} and X_{Lg} represent the capacitor and inductor impedance under given switching frequency. Capacitance value might be chosen as:

$$X_{cf} = \left(\frac{1}{10} \sim \frac{1}{5}\right) X_{Lg} \tag{8}$$

Too large choose of filter capacitor impedance X_{cf} will force much more higher frequency current component flows to the grid, poor harmonic absorption performance would be obtained. On the other hand, Smaller choose of filter capacitor impedance, which means large filter capacitance value, will allow much of the reactive current component flows through the capacitor. Power consumption of the LCL filter will increase. Hence, the fundamental reactive power absorbed by the capacitor should not be greater than 5% of the system's rated active power, which means:

$$C_f \le \frac{\lambda P}{3 \times 2\pi f_1 E_m^2} \tag{9}$$

Where in (9), P is the rated output power of grid connected inverter, E_m is the root mean square values (RMS) of grid connected phase voltage, f_1 is the fundamental frequency of the grid, λ is the ratio of fundamental power absorbed by the filter capacitor to total power. Based on the aforementioned content, considering about the current accuracy test requirement of PABTS, the maximum allowable current ripple is specified as the 2% of the peak phase current value, inverter side inductance value L_{inv} could be calculated according to maximum current ripple limitation given in [17]:

$$\Delta i_{L\_inv,\max} = \frac{1}{8} \cdot \frac{V_{dc}}{L_{inv} \cdot f_{sw}} = 2\% \cdot i_{rated} \tag{10}$$

Where in (10), i_{rated} is the inverter rated current, f_{sw} is the switching frequency of the power IGBT, and v_{dc} is DC-bus voltage, respectively. In this paper, we chose v_{dc}=900V, f_{sw} =10 kHz, and i_{rated}=400A, therefore, the inverter side inductance value is L_{inv} =5.21mH.

As analyzed in the former part, it would be a proper value if the ratio between inverter side inductance and converter side could be chosen 4~6, filter capacitor C_f could be chosen a little bit larger in order to save magnetic core material, in this paper, a value of L_{inv}/L_g=5 is selected, grid side inductance L_g would be 1mH. Considering about the capacitor selection principle in (8), coefficient between grid side inductance L_g and capacitance C_f is chosen as 0.125, combined with the switching frequency 10 kHz, the filter capacitance could obtained with a value of 20uF.

As a conclusion, parameters of the LCL filter are summarized as:

$$L_{inv}=5.2\text{mH},\ L_g=1\text{mH},\ C_f=20\text{uF}$$

Combined with dc-link voltage, switching frequency, and current ripple requirement, the parameters of the inverter/rectifier side could be listed in Table.1 in the appendix. In the next chapter, we will discuss the selection of inductance for the dc-dc buck and boost chopper.

3.4 Inductance of the boost chopper

In order to keep the discharging test current stable, the duty cycle of the dc-dc converter is regulated correspondingly. However, as the influence caused by the parasitic resistance boosts the inductance, the output voltage will drop when the duty cycle surpasses a certain value. Therefore, a smaller parasitic resistance of inductance should be chosen for the boost chopper, and the duty cycle is usually limited to μ<0.88. Using the principle of energy conservation equation, we can obtain the relationship between the discharging energy and the output dc-link output energy by:

$$P_{RL} = I_{RL} \cdot V_{dc} = V_{\text{bat}} \cdot I_{bat} \Rightarrow \frac{I_{RL}}{I_{bat}} = \frac{V_{bat}}{V_{dc}} = 1 - D \tag{11}$$

where in (11), I_{bat} and I_{RL} symbolize the average current of the battery input and the load current on the DC bus, respectively. Since V_{L}=L·di/dt, we obtain:

$$\Delta i_L = V_{bat} \cdot DT_s / L \tag{12}$$

In (12), Δi_{L} is the input current ripple, T_{s} is the PWM cycle for the power transistors in the boost converter. L is filter inductance in the boost chopper. Defining the current ripple coefficient as η=Δi_{L}/i_{L}, we will get the relationship between inductance value and dc-link voltage, duty cycle, input power, and current ripple coefficient, which is shown as:

$$L = \frac{(1-D)^2 DV_{dc}^2 T_s}{\eta P_{RL}} \tag{13}$$

The maximum filter inductance value L for dc-dc buck and boost chopper can be obtained by using dL/dt=0, when D=1/3 from (13):

$$L_{\max} = \frac{4V_{dc}^2 T_s}{27\eta P_{RL}} \tag{14}$$

From (14), we know that the inductance of the boost chopper is decided by the dc-link voltage, the current ripple coefficient, and the output power capability requirement. In order to satisfy the requirement of the current ripple on the rated parameters, the inductance value needs to be chosen to satisfy following requirement:

$$L >= L_{\max} \tag{15}$$

In the proposed scheme, a value of 2mH, by choosing η=0.05, is chosen for the inductance for experiment, which is based on the required parameters shown in Table 1 in the appendix.

3. Control Strategy of the System

Fig. 9 offers the block diagram of power converter topology and its implementation on energy recovery PABPTS. Unlike conventional power converter, such as VSC (voltage source converter)-based grid connected or CSC (current source converter)-based grid connected systems, power isolation in high power battery testing instruments is stringent required. Mathematics and current controller have been illustrated in former work and are shown in [9]. Moreover, in the composite power converter, the dc-link voltage is not directly controlled, and is charged by the discharging current from dc-dc power converter. In this chapter, we will first analyze the estimation of instantaneous active and reactive power, then, control strategy of the whole system will be illustrated.

4.1 Instantaneous active and reactive power estimator

Since, active and reactive power of the system should be controlled, respectively. An important part of the proposed PABPTS is the active and reactive power estimation. Instantaneous active power (p) and reactive power (q) are estimated by (16) and (17), respectively. Active power is the scalar product of the current and the voltage, and the reactive power q is calculated as a vector product of the current and voltage.

$$p\_dq = \frac{3}{2} \cdot \left(v_d^* \cdot i_{d\_fill} + v_q^* \cdot i_{q\_fill} \right) \tag{16}$$

$$q\_dq = \frac{3}{2} \cdot \left(v_q^* \cdot i_{d\_fill} - v_d^* \cdot i_{q\_fill} \right) \tag{17}$$

From (16) and (17), current reference for the specified active and reactive power are:

$$i_d^* = \frac{2}{3} \cdot \frac{\left(p_{ref} \cdot v_d + q_{ref} \cdot v_q \right)}{v_d^2 + v_q^2} \tag{18}$$

$$i_q^* = \frac{2}{3} \cdot \frac{\left(p_{ref} \cdot v_q - q_{ref} \cdot v_d \right)}{v_d^2 + v_q^2} \tag{19}$$

Where v_{d}, v_{q}, $i_{\text{d\_fill}}$, and $i_{\text{q\_fill}}$ are the voltages and currents under dq coordinates, respectively.

4.2 Composite power converter control for PABPTS

Based on the requirements mentioned in the introduction part, control strategy of the composite power converter for PABTS is shown in Fig. 9. The system has three current loops, two of them are active and reactive current loop. Reference current is generated by (18) and (19) in 4.1. Another loop is the current loop in the boost chopper, which should be functioned as current source. what is more,

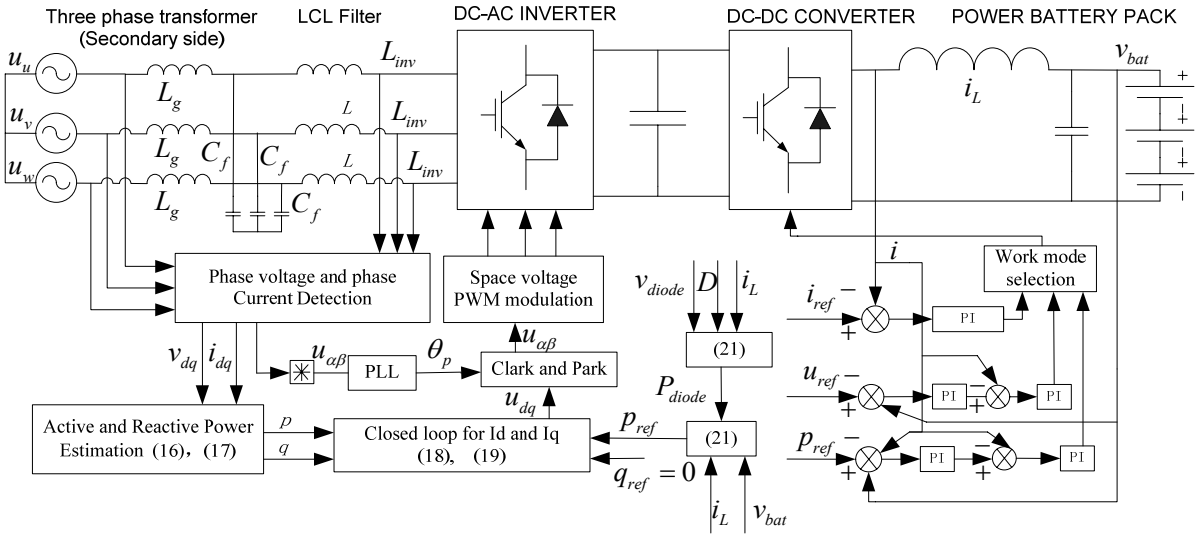

Fig. 4. Power circuit and implementation of the grid connected energy recovery PABPTS with Δ-Y transformer.

PABPTS requires wide range, high resolution discharging and charging currents, fast response, and minimum steady state error. This function is used for mimicking the instantaneous startup and driving process in electric vehicle applications. Active and reactive power reference, which is integrated to the grid, is derived from the energy released from power battery pack. Active power reference in ac side varies up and down with the discharging current and terminal voltage of power battery pack.

In order to reduce the sensors in the PABPTS, active power for integrating to grid could be indirectly calculated by the released battery power and power loss on the bypass diode in the upper IGBT, which could be calculated as:

$$P_{diode} = v_{diode} \cdot (1 - D) \cdot i_L \tag{20}$$

Where in (20), v_{diode} is voltage drop on the bypass diode, D is the duty cycle of boost chopper, i_L symbols the feedback inductance on the dc-side, which is the discharging current reference in boost modulation. Hence, the active power reference P in the inverter side would be:

$$P = v_{bat} \cdot i_L - P_{diode} \tag{21}$$

Usually, conventional direct power control (DPC) uses a switching table for PWM output signal generation, which is adopted according to the sign of active Δp and reactive Δq power difference. This paper adopts two proportional-integral (PI) controllers combined with space voltage pulse width modulation (SVPWM) to overcome the un-fixed switching frequency and to improve the utilization of dc-link voltage. The recommended scheme could realize minimum steady state error. In Fig. 9, A synchronous reference frame transformation is applied, where the angle information is provided by the phase-locked loop (PLL) to guarantee correct operation even under grid voltage distortion. The main advantage of using a current source instead of a voltage source is that within the control frequency range, higher output impedance is observed from the point of view of the grid voltage. This minimizes the effect of voltage harmonics on the output current and improves the power quality.

5. Simulation Verification

In order to confirm the effectiveness of the proposed system, simulations are conducted with PSim based on the system shown in Fig. 9. The steady state and dynamic performance of the proposed system are illustrated. Electrical parameters for the simulation model are given in Table 1. The simulation study is performed with two main objectives in mind:

- To demonstrate the validity and feasibility of the proposed control scheme.
- To measure the dynamic performance of the PABPTS, including the discharging current response, active and reactive power responses, and harmonics of the grid current and voltage.

Initial dc-link capacitor voltage is set with 500V for pre-charge. Dc-link voltage is set to 900V as a prerequisite for starting SVPWM modulation. The simulated waveforms of discharging current vs. reference current for PBPTS are shown in Fig. 10, Gain and time constant of the PI controller in discharging current are chosen as: k_p=0.02, T=0.015. A step forward current reference is given at 30ms from 0A to 200A, and at 80ms from 200A to 400A. A step down current is given at 130ms from 400A to 200A, The results show an output delay of 70ms to enter steady state at the first step-up rising time. and the second step-up

results show a fast response combined with nearly 10A overshot and finally reaches the reference value. A sharp dc-link current occurs when discharging current changes from 400A to 200A, this is caused by the surging current from the dc-side inductor. Simulation results shows that the feedback current follows reference current very well.

Fig. 11 shows the time response of the active power P and reactive power Q, respectively. We can see that active and reactive power estimation results towel agrees with the reference power. reactive power reference is set to zero to ensure an unity power factor control. Active and are not directly controlled; active power component is supplied by (21) in 4.2. Fig. 11 also show that when a step-down reference current is given, A resonance between active and reactive power would occur, and the oscillation time is about 2ms from 400A to 200A, which was caused by vibrations between the dc-link capacitor and inductor.

Fig. 12 shows time response of phase current i_a and phase voltage v_{an} when grid-connected. It can be seen that the grid current is almost in phase with grid voltage. Comparison results for L and LCL filter have been shown in Fig. 13. The current total harmonic distortion for L filter is 3.18% and for LCL filter is 2.24%, which demonstrates better performance on harmonic attenuation when using

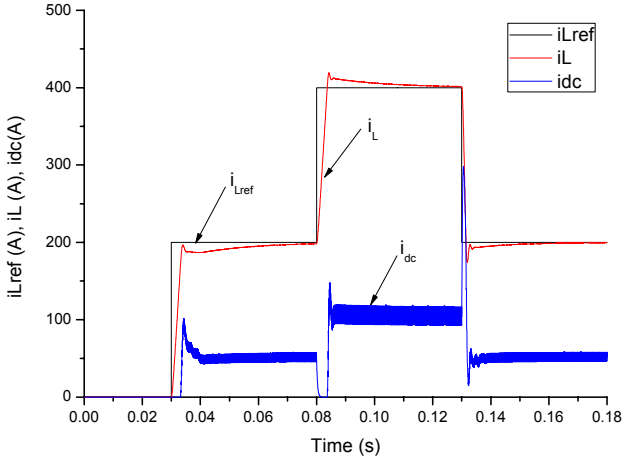

Fig. 10. Simulation results of power battery pack discharging current vs. reference discharging current.

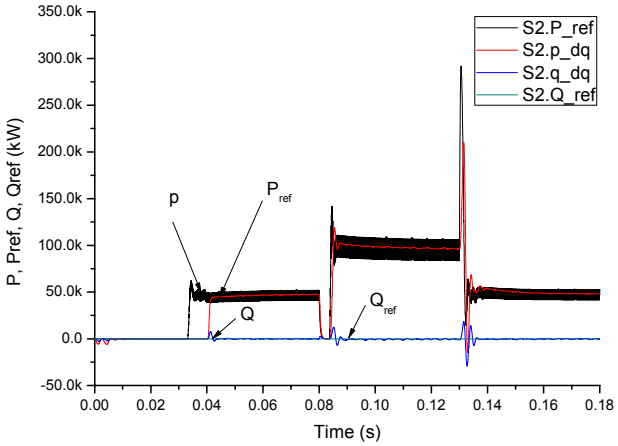

Fig. 11. Simulation results of active power response vs. reference active power.

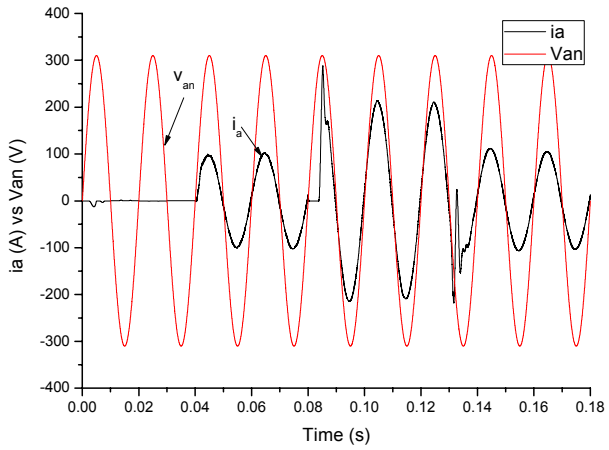

Fig. 12. Phase voltage and phase current under charging discharging current.

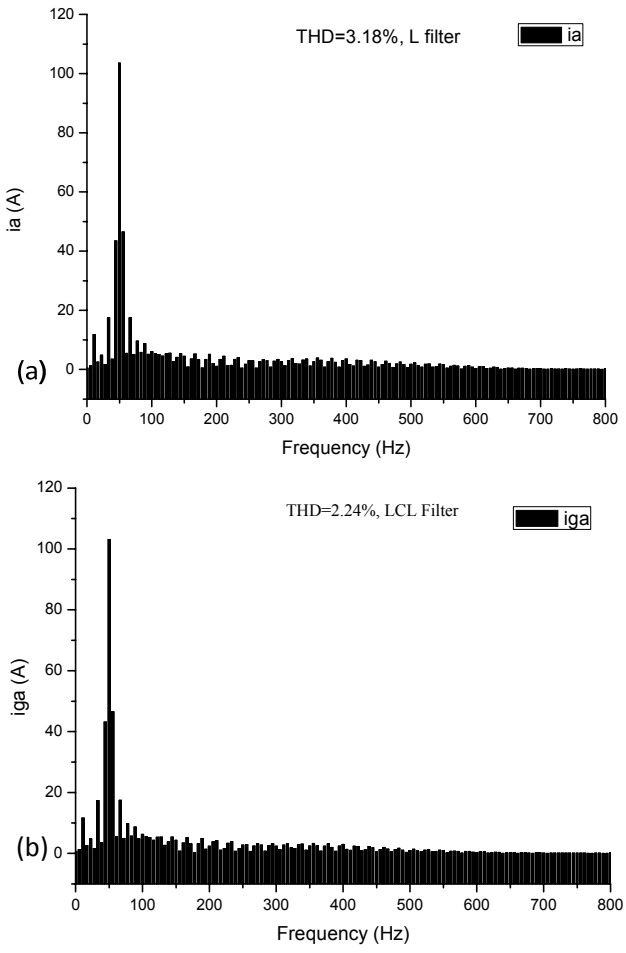

Fig. 13. FFT of phase current with L filter (a) and LCL filter (b) at f=50Hz.

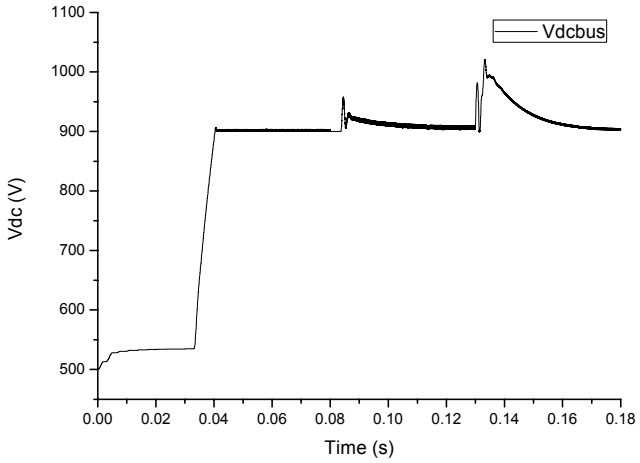

Fig. 14. Response of current and voltage reference under constant discharging current control on the DC-bus.

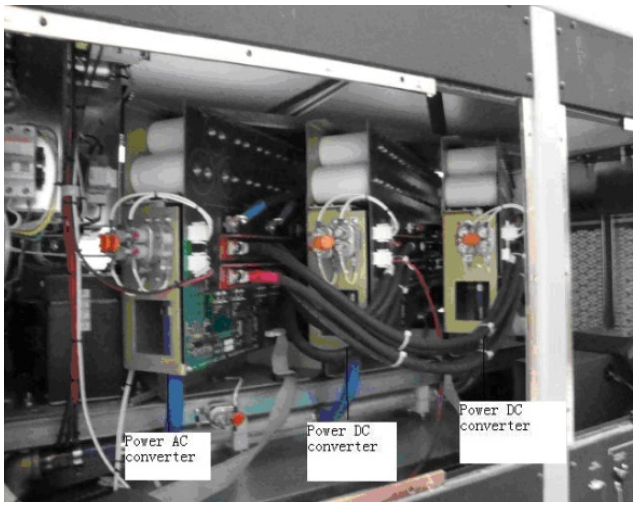

Fig. 15. Two-channel energy recovery PBPTS prototype for experiment.

LCL filter.

Fig. 14 shows time response of dc-link voltage. It could be found that dc-link voltage v_{dc} is well maintained at 900V at the first step-forward current reference. When the second step forward voltage is given, a peak voltage with 50V occurs, and finally is convergent to 900V again after 70ms later. Fig. 14 also shows that whenever a step down current reference is put forward (from 400A to 200A), An inrush dc-link voltage occurs, this is equivalent to a reduced load on the inverter side, And again convergent to 900V after 50ms later.

As a result, we could conclude that the suggested power circuit and it corresponding control strategy for energy recovery PABPTS are feasible and applicable.

6. Experiments

6.1 Experimental system configuration

A 175kW power converter experimental prototype is developed in order to examine the operating characteristics of the proposed technique. Power circuit of the PWM converter consists of an insulated gate bipolar transistor (IGBT/SKM400GB-128D)-based full-bridge circuit and a half-bridge circuit, Electrical parameters used in experiment are shown in Table 1. Two Hall-effect LEM sensors (LT108-S7) and four isolation voltage sensors are employed for line currents and DC-link voltage detection, respectively. In the dc-dc power circuit part, one high-resolution LEM sensor is employed for the charging and discharging currents acquisition. Estimation of the instantaneous power and voltages is realized by using a DSP (TMS320LF2407A-40MHz) from Texas Instrument. The estimation program is executed in every 9μs control period, which is initiated by an internal timer. A total of eight PWM output signals are required in the proposed scheme. Two of them are used for the buck-boost chopping, and the other six are used for the space voltage PWM modulation. Fig. 15 shows the hardware setup of energy recovery PABPTS, which is composed of two independent channel dc-dc choppers and one AC-DC converter.

6.2 Experimental results and analysis

Based on the simulations above, several experimental tests are conducted to verify the feasibility of the proposed technique. Fig. 16 shows the experimental result under constant charging current test operation from 0A to 120A with the given current reference. Maximum and minimum currents are shown, and it could be seen that the proposed nonlinear-controller provides better performance after linear error compensation. Fig. 17 shows the step response of the waveform under reference current and measured current, which shows that the measured current could keep

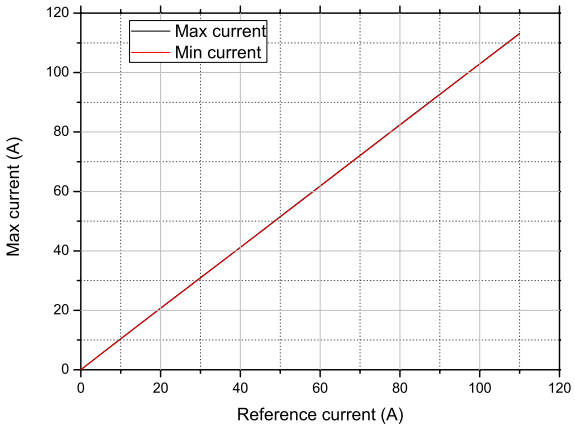

Fig. 16. Waveform of feedback charging current and reference current.

track of the reference with high accuracy and fast response. Rising times are nearly 75 ms from 0A to 400A and 35ms from 400A to 800A. However, large overshot exists in the transient process, which is caused by the near-zero capacitor voltage on the DC-link in initial state. The larger the inductance of the boost chopper is, the smaller the inrush current would be. This could be solved by pre-charging the dc-link power capacitors before experiment. In addition, as is shown in Fig. 17, a resonance exists in the step-down current reference, which may be caused by dc-dc side inductor *L* and dc-link capacitor *C*, where energy exchanges to and from *L* and *C*, and finally reaching a steady state. The resonance time is nearly 0.25ms from 800A to 400A.

Fig. 18 illustrates the estimated active power P and reactive power Q for a step forward change from 0 to 120kW at 0.3s, and from 120kW to 240kW at 1ms.The estimated average reactive power maintains zero because

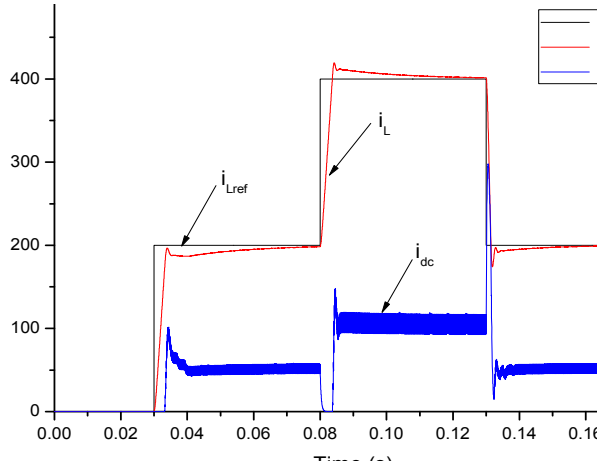

Fig. 17. Time response of battery pack current.

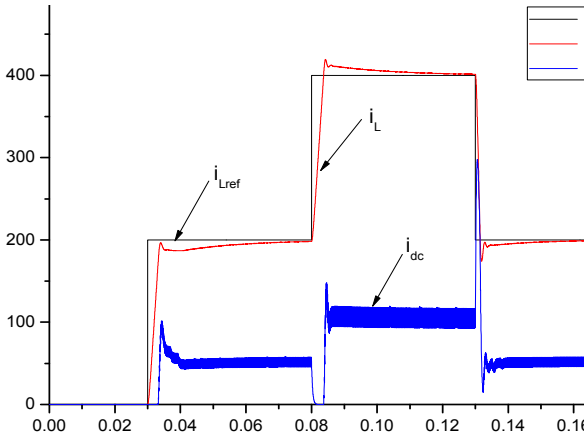

Fig. 18. Response of active and reactive power for a step change from 0 to 120kw at 0.3s, from 120kw to 240kw at 1ms.

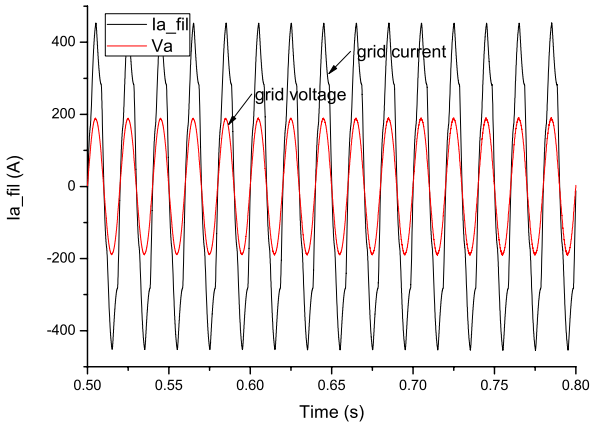

Fig. 19. Waveform of measured grid connected current and voltage.

of the unity power factor operation. The active power reference derives from the discharging energy in the DC-DC converter.

Fig. 19 illustrates the grid current and voltage. It could be seen, the grid current is not ideal sinusoidal and has some even harmonics. It is likely that the even harmonics are a result of program delays during execution, dead time, or suppression of pulses. We can observe that the grid current is almost in phase with grid voltage, and unity power factor operation is successfully achieved.

7. Conclusions

This paper proposes a Δ-Y interface transformer-based composite power circuit with an LCL filter for energy recovery PAPABTS. Corresponding control strategy has been put forward. Parameter design procedure and principle of LCL filter have been analyzed and proposed, respectively. An improved way of dc-link voltage and current detection sensor reduction is illustrated. In addition, switching method of integrating or non-integrating to power grid is used to maintain dc-link voltage constant. he Feasibility of the proposed system was examined through experimental tests using a 175kW prototype. Results show that the proposed system makes it possible to obtain high accurate charging and discharging current test experiments, which recovers energy with nearly unity total power factor. In addition, Fast response and excellent stability of the discharging currents in the power battery pack are confirmed.

It is suggested that future work might be focused on extending two-level converter to multi-level converter in order to further reduce current harmonic in all ranges.

Appendix

Table 1. Simulation and experiment parameters

Elements	Parameters	Value
Power Battery Pack	Battery voltage V_{bat}	240V
	Battery number	20
	Battery capacity	12V/200AH
AC Power grid	Grid voltage (line to line rms) V_g	230V
	Line frequency f_n	50Hz
	Grid impedance L_g	0.2mH
Transformer	Resistance of the primary winding	1mΩ
	Resistance of the secondary winding	1mΩ
	Leakage Inductance of the primary winding L_p	10uH
	Leakage inductance of the secondary winding L_s	10uH
	Magnetizing inductance seen from the primary winding	0.5mH
	No. of turns of the primary winding n_p	150
	No. of turns of the second winding n_s	100
LCL filter	Grid side inductor L_g	1mH
	Converter side inductor L_{inv}	5.2mH
	Filter capacitor C_f	20uF
DC-DC converter	Nominal power	175kW
	Inductor used in boost chopping L	2mH
	Switching frequency	1500Hz
	Dead time t_d	2us
DC-AC converter	Nominal power	175kW
	DC-link capacitor C_{dc}	5500uF
	IGBT switching frequency f_{inv}	10kHz
	Dead time t_d	2us

Acknowledgments

This work was supported by the Fundamental Research Funds for the Central Universities of China (NO. ZYGX 2012J095), and also supported by the National Research Foundation of Korea (NRF) grant funded by the Korea government (MEST) (No. 2012-038978).

References

[1] L. Zhang, W. Kang, L. Jia, M. Zhao, and R. Xu, "Control of Bidirectional Current Source SVPWM Converter in the Power Accumulator Battery Testing System," in *Power and Energy Engineering Conference (APPEEC), 2010 Asia-Pacific*, 2010, pp. 1-4.

[2] N. J. Fellner C, "High.power batteries for use in hybrid vehules," *Power Sources,* vol. 85(1):229-236., 2000.

[3] Y. Xiangwu, D. Chunlin, L. Heming, Z. Lixia, and W. Fang, "Application of three-phase current source converter in power battery testing system for electric vehicles," in *Electrical Machines and Systems, 2008. ICEMS 2008. International Conference on*, 2008, pp. 4205-4209.

[4] G.-c. Li and H.-y. Wang, "Study on Fuzzy Control in Power Battery Testing System," in *Control and Automation, 2007. ICCA 2007. IEEE International Conference on*, 2007, pp. 1110-1112.

[5] J. Gill, "Advanced EV/HEV battery pack testing using the ABC-150 power system," in *Battery Conference on Applications and Advances, 1997., Twelfth Annual*, 1997, pp. 127-131.

[6] H. Kobayashi, M. Shikano, S. Koike, H. Sakaebe, and K. Tatsunii, "Investigation of positive electrodes after cycle testing of high-power Li-ion battery cells I. An approach to the power fading mechanism using XANES," *Journal of Power Sources,* vol. 174, pp. 380-386, Dec 6 2007.

[7] B. Schweighofer, K. M. Raab, and G. Brasseur, "Modeling of high power automotive batteries by the use of an automated test system," *Instrumentation and Measurement, IEEE Transactions on,* vol. 52, pp. 1087-1091, 2003.

[8] M. Uno and K. Tanaka, "Accelerated Charge-Discharge Cycling Test and Cycle Life Prediction Model for Supercapacitors in Alternative Battery Applications," *Industrial Electronics, IEEE Transactions on,* vol. 59, pp. 4704-4712, 2012.

[9] B. Long, Z. Xian, S. T. Lim, and K. T. Chong, "Design of Energy Recovery Power Battery Pack Testing System," *International Review of Electrical Engineering-Iree,* vol. 7, pp. 4672-4683, Jul-Aug 2012.

[10] L. Fei, Z. Yan, D. Shanxu, Y. Jinjun, L. Bangyin, and L. Fangrui, "Parameter Design of a Two-Current-Loop Controller Used in a Grid-Connected Inverter System With LCL Filter," *Industrial Electronics, IEEE Transactions on,* vol. 56, pp. 4483-4491, 2009.

[11] H. Mahmood and J. Jin, "Modeling and Control System Design of a Grid Connected VSC Considering the Effect of the Interface Transformer Type," *Smart Grid, IEEE Transactions on,* vol. 3, pp. 122-134, 2012.

[12] X.-Q. Guo, W.-Y. Wu, and H.-R. Gu, "Modeling and simulation of direct output current control for LCL-interfaced grid-connected inverters with parallel passive damping," *Simulation Modelling Practice and Theory,* vol. 18, pp. 946-956, 2010.

[13] G. Tsengenes, T. Nathenas, and G. Adamidis, "A three-level space vector modulated grid connected inverter with control scheme based on instantaneous power theory," *Simulation Modelling Practice and Theory,* vol. 25, pp. 134-147, 2012.

[14] J. H. Lee, H. G. Jeong, and K. B. Lee, "Performance Improvement of Grid-Connected Inverter Systems under Unbalanced and Distorted Grid Voltage by Using a PR Controller," *Journal of Electrical Engineering & Technology,* vol. 7, pp. 918-925, Nov 2012.

[15] J. H. Lee, D. Y. Jung, T. K. Lee, Y. R. Kim, and C. Y. Won, "Regenerative Current Control Method of Bidirectional DC/DC Converter for EV/HEV Application," *Journal of Electrical Engineering & Technology,*

vol. 8, pp. 97-105, Jan 2013.
[16] M. A. Abusara and S. M. Sharkh, "Design and Control of a Grid-Connected Interleaved Inverter," *Power Electronics, IEEE Transactions on,* vol. 28, pp. 748-764, 2013.
[17] J. Muhlethaler, M. Schweizer, R. Blattmann, J. W. Kolar, and A. Ecklebe, "Optimal Design of LCL Harmonic Filters for Three-Phase PFC Rectifiers," *Power Electronics, IEEE Transactions on,* vol. 28, pp. 3114-3125, 2013.

Long Bo received B.S. and M.S. degrees from Petroleum University, Xian, in 2001 and 2004, then, received his Ph.D. from Xi'an Jiao Tong University in June, 2008. He is currently a full-time lecturer in the school of Mechatronic Engineering at the University of Electronic Science and Technology of China, in ChengDu. His current research interests include high-performance motor drives, renewable energy generation, distributed generation systems, micro-grid, and unified power quality conditioners. He is currently doing post doctorate work in the Department of Electric and Information Engineering at Chonbuk National University, Jeonju, in South Korea.

Kil To Chong received his Ph.D. in Mechanical Engineering from Texas A&M University in 1995. Currently, he is a professor and department head of the School of Electronics and Information Engineering, and he is a member and head of the Advanced Electronics and Information Research Center at Chonbuk National University in Jeonju, Korea. His research interests are in the areas of motor fault detection and control, network system control, sensor network systems, time-delay systems, and neural networks.